Experiment: Ridge-waveguide DFB lasers with a MQW active region have been fabricated by a two-step metal organic chemical vapour deposition (MOCVD) process. The choice of the grating depth has resulted in the removal of four out of six quantum wells. From transmission electron micrographs of the grating, the duty factor of an equivalent rectangular-wave grating has been estimated to be 76.4% ± 2%. Bars of DFB lasers have been cleaved with cavity lengths of 305 and 380 μm, and antireflection coatings ($R < 0.2\%$) have been applied to both facets. Chips of each cavity length have been soldered with the junction-side up onto diamond heatsinks with ceramic submounts.

Fig. 2 shows the power against wavelength spectrum at a submount temperature of 20°C for a 305 μm laser, from which the light has been collected with an Ando AQ6317 optical spectrum analyser set to a resolution of 20 pm. Singlemode oscillations have been observed over the whole bias range, with a 305 μm laser sidemode suppression ratio (SMSR) improving from 59.1 dB at 50 mA bias to 64.7 dB at 200 mA, and a 380 μm laser SMSR improving from 59.1 dB to 63.3 dB over the same current range. All lasers that have been measured from this wafer have an SMSR > 60 dB at 200 mA. The stopband width of these lasers indicates that $\kappa_{real} \simeq 130\,cm^{-1}$, implying κL products of ~4 and ~5 for the shorter and longer DFB cavity, respectively. The light against current characteristic at a submount temperature of 20°C from one laser facet is plotted in Fig. 3 for a 305 and a 380 μm laser.

Dynamic properties: The relaxation oscillation frequency f_{relax} and damping Γ have been determined by fitting the relative intensity noise (RIN) function to

$$RIN = \frac{A + Bf^2}{\left(f_{relax}^2 - f^2\right)^2 + (\Gamma/2\pi)^2 f^2}$$

The RIN has been measured using an HP electrical spectrum analyser with a 1550 optical head (HP-70810B lightwave section plugin, HP-70908A precision frequency reference module, HP-70900B local oscillator module, and HP-70004A controller in an HP-70001A mainframe) covering a range from 150 MHz to 20 GHz. An HP supplied program for the HP-70004A controller extracts the shot and thermal noise from the RIN. Room-temperature measurements have been made with −1.6 dBm of light coupled through a tapered fibre at 60 mA bias, which provides sufficient power to accurately measure the RIN without saturating the detector. An ILX Lightwave LDC-3900 modular laser diode controller supplied a low noise DC bias current from 20 to 120 mA. The dynamic figures of merit, D, Γ_0, and K, have been extracted over this current range by fitting to $f_{relax}^2 = D(I - I_{th})$ and $\Gamma = \Gamma_0 + Kf_{relax}^2$.

Typical values for 305 and 380 μm cavities with both facets AR-coated are: D = 1.4 to 1.7 GHz/mA$^{1/2}$; K = 0.31 to 0.36 ns; and Γ_0 = 8.9 to 19 ns^{-1}. These results compare favourably with previous first-order in-phase gain-coupled grating studies [8]. Dynamic benefits of gain- over index-coupled gratings include more open eye diagrams and enhanced dynamic performance [2]. The large values of Γ_0 that have been obtained indicate these benefits are also realisable in truncated well second-order gain-coupled lasers.

Conclusion: In-phase gain-coupled multiple quantum well 1.55 μm DFB lasers with second-order gratings have been fabricated by a two-step MOCVD process. Lasers with a κL value between 4 and 5 with both facets AR-coated have achieved a sidemode suppression ratio > 63 dB and power > 25 mW from one facet when biased at 200 mA. Dynamic damping rates have been found to be comparable to values obtained for truncated well GC-DFBs with first-order gratings.

Acknowledgments: The authors thank C. Miner, J. Valerio, S. Clements and A.G. Self for their guidance.

25 September 2001
Electronics Letters Online No: 20011020
DOI: 10.1049/el:20011020

D.M. Adams, I. Woods, J.K. White, R. Finlay and D. Goodchild (*Nortel Networks, High Performance Optical Component Solutions, 3500 Carling Avenue, Ottawa, ON, K2H 8E9, Canada*)

E-mail: kenton@nortelnetworks.com

References

1 DAVID, K., MORTHIER, G., VANKWIKELBERGE, P., BAETZ, R., WOLD, T., and BORCHERT, B.: 'Gain-coupled DFB lasers versus index-coupled and phase-shifted laser: a comparison based on spatial hole burning corrected yield', *IEEE J Quantum Electron.*, 1991, **27**, (6), pp. 1714–1723

2 YANG, S., WILLIAMS, K., PLENTY, R.V., WHITE, I.H., WOODS, I., and WHITE, J.K.: 'Enhanced performance of uncooled srongly-gain-coupled MQW DFB lasers in 10 Gb/s link applications'. Proc. ECOC 2001 Conf., Amsterdam, Holland, 2001, Paper Tu.B.1.4

3 MAKINO, T., LU, H., and LI, G.P.: 'Transfer-matrix dynamic model of partly gain-coupled 1.55μm DFB lasers with a strained layer MQW active grating', *IEEE J. Quantum Electron.*, 1994, **30**, (11), pp. 2443–2448

4 CHAMPAGNE, A., MACEIJKO, R., and MAKINO, T.: 'Enhanced carrier injection efficiency from lateral current injection in multiple-quantum well DFB lasers', *IEEE Photonics Technol. Lett.*, 1996, **8**, (6), pp. 749–751

5 SHAMS-ZADEH-AMIRI, A.M., HONG, J., LI, X., and HUANG, W.-P.: 'Second- and higher order resonant gratings with gain or loss – part I: Green's function analysis', *IEEE J. Quantum Electron.*, 2000, **36**, (12), pp. 1421–1430

6 SHAMS-ZADEH-AMIRI, A.M., HONG, J., LI, X., and HUANG, W.-P.: 'Second- and higher order resonant gratings with gain or loss – part II: Designing complex-coupled DFB lasers with second-order gratings', *IEEE J. Quantum Electron.*, 2000, **36**, (12), pp. 1431–1437

7 KAZARINOV, R., and HENRY, C.H.: 'Second-order distributed feedback lasers with mode selection provided by first-order radiation losses', *IEEE J. Quantum Electron.*, 1985, **21**, (2), pp. 144–150

8 WHITE, J.K., BLAAUW, C., FIRTH, P., and AUKLAND, P.: '85°C investigation of uncooled 10 Gbit/s directly modulated InGaAsP RWG GC-DFB lasers', *Photonics Technol. Lett.*, 2001, **13**, (8), pp. 773–775

Conformal mapping for buried CPW with finite grounds

D. Jessie and L. Larson

An analytic expression for the effective dielectric constant and impedance of a coplanar waveguide with finite grounds and embedded in a dielectric (ECPWFG) has been developed for the first time. Limiting examples of the expression are compared to known accurate results for standard CPW structures, of which excellent agreement is obtained.

Introduction: Coplanar waveguide (CPW) type structures have been studied extensively since first described as a transmission line system by C.P. Wen in 1969. Many variations have been investigated [1 – 4], but for the first time a closed-form expression is given for a CPW structure with finite grounds, buried in a dielectric, conductor backed, and having finite conductor thickness (ECPWFG).

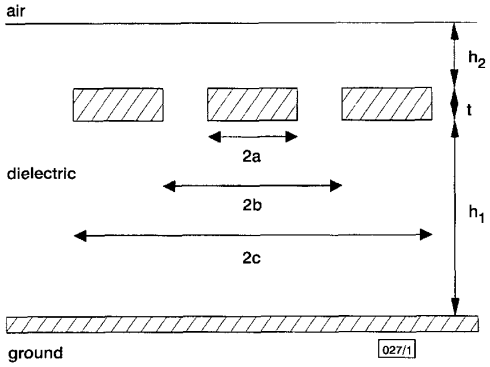

Fig. 1 *ECPWFG cross-section*

The general layout of the transmission line system is shown in Fig. 1. The dielectric height extends from the grounded plane at

the bottom to above the conductors ($h1 + t + h2$). The conductor pitch is $b + a$. The two outside conductors are grounded to the backplane conductor below. To obtain the impedance of the transmission line, the ratio of capacitances with dielectrics present to capacitances with all dielectrics replaced with air must be calculated.

The capacitances per unit length for the ECPWFG line are as follows: Capacitance $C1$ is the capacitance of the top face of the conductors where the electric field lines are contained partially in the dielectric and partially in the air. Capacitance $C2$ is the parallel plate capacitance between the conductors due to finite metal thickness. Capacitance $C3$ is due to the electric fields on the bottom face of the conductors.

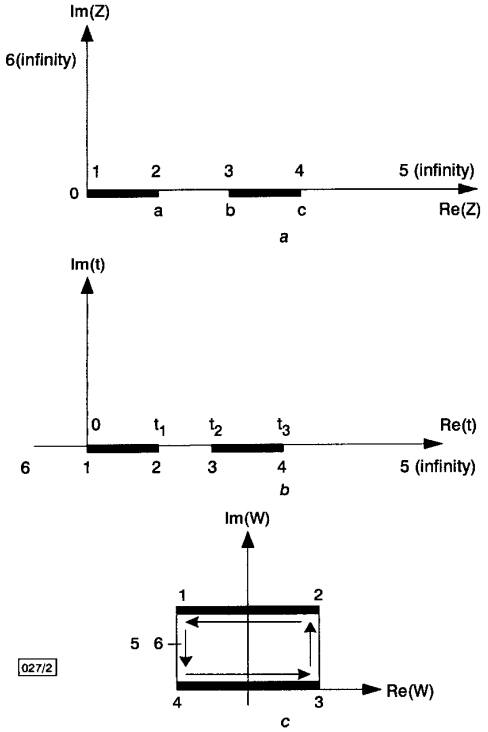

Fig. 2 *Conformal mapping of top face of ECPWFG without dielectric*
a Z-plane
b Intermediate stage in *t*-plane
c Parallel-plate capacitor in *W*-plane

Theory: Following a similar method to that of [4], Fig. 2 shows the progression from the Z-plane, to an intermediate stage in the t-plane, and finally to a parallel-plate capacitor in the W-plane.

The transformation equation for the configuration with only air above the interface is given by

$$t = z^2 \tag{1}$$

The Schwarz-Christoffel integral is then

$$W = \int_{t_i}^{t_j} \frac{dt}{\sqrt{t(t-t_1)(t-t_2)(t-t_3)}} \tag{2}$$

with indices given by $t_1 = a^2$, $t_2 = b^2$ and $t_3 = c^2$.

The capacitance per unit length is then

$$C1_a = 2\epsilon_o \frac{\widetilde{12}}{\widetilde{23}} = 2\epsilon_o \frac{K(k_{1a})}{K'(k_{1a})} \tag{3}$$

where $\widetilde{ij}$ signifies integration over the distances i and j denoted in Fig. 2. The argument $k_1 a$ is

$$k_{1a} = \frac{a}{b}\sqrt{\frac{1-\frac{b^2}{c^2}}{1-\frac{a^2}{c^2}}} \tag{4}$$

K and K' are solutions to the complete elliptic integrals of the first kind and its complement, respectively.

The formulation with dielectric present above the conductors is similar to that derived with the exception of the dielectric thickness $h2$ is transformed into a unity offset from the origin. The transformation equation for the configuration with $\epsilon \neq 1$ dielectric above the interface is given by [5]

$$t = \cosh^2\left(\frac{\pi z}{2h_2}\right) \tag{5}$$

where the hyperbolic function includes the effect of the boundary at $h2$.

The capacitance per unit length is then

$$C1_d = 2\epsilon_o(\epsilon_r - 1)\frac{K(k_{1d})}{K'(k_{1d})} \tag{6}$$

and the argument $k_1 d$ is

$$k_{1d} = \frac{\sinh\left(\frac{\pi a}{2h_2}\right)}{\sinh\left(\frac{\pi b}{2h_2}\right)}\sqrt{\frac{1-\frac{\sinh^2\left(\frac{\pi b}{2h_2}\right)}{\sinh^2\left(\frac{\pi c}{2h_2}\right)}}{1-\frac{\sinh^2\left(\frac{\pi a}{2h_2}\right)}{\sinh^2\left(\frac{\pi c}{2h_2}\right)}}} \tag{7}$$

The total capacitance above the dielectrics is then $C1_a + C1_d$ [5].

The calculation of $C3$ is similar to the derivation of $C1$. The transformation for the configuration with only dielectric below the interface is the same as eqns. 5 – 7, with $h2$ replaced by $h1$ and ϵ_r replacing $\epsilon_r - 1$.

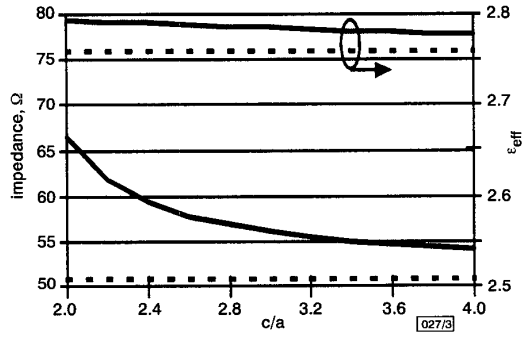

Fig. 3 *Results for c varied, b = 18 mil, a = 10 mil*
——— ECPWFG
– – – – CPW

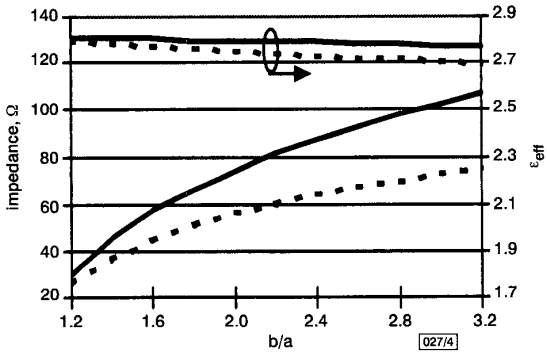

Fig. 4 *Results for b varied, a = 10 mil, c = b + 2 mil*
——— ECPWFG
– – – – CPW

The capacitance due to finite metal thickness $C2$ is calculated by the classic parallel plate capacitor formula, since the fringing fields at the top and bottom faces of the conductors are contained in the above derivations. They will be denoted $C2_a$ for the air case and $C2_d$ for the dielectric case.

The impedance can be calculated with all known capacitances understood. The effective dielectric constant is then

$$\epsilon_{eff} = \frac{C}{C^a} = \frac{C1_a + C1_d + C3_d + C2_d}{C1_a + C3_a + C2_a} \tag{8}$$

The impedance is then calculated by

$$Z_0 = \frac{1}{v\sqrt{\epsilon_{eff}}C^a} \quad (9)$$

where v is the speed of light in vacuum.

Results: Fig. 3 compares the ECPWFG ϵ_{eff} and Z_0 from eqns. 8 and 9 with embedded CPW structure [5] (note that the value of c extends to infinity). The top curve shows ECPWFG change in ϵ_{eff} for $h1$ = 40 mil, $h2$ = 28 mil, a = 10 mil, b = 18 mil, t = 4 mil, as c is varied from 20 to 40 mil. The bottom curve shows the values for Z_0.

In Fig. 4, the same equation given by [5] of an embedded CPW structure with c value extending to infinity is plotted against eqns. 8 and 9 for narrow values of c while b is varied. The values used are $h1$ = 40 mil, $h2$ = 28 mil, a = 10 mil, $c = b + 2$ mil, t = 4 mil, and b is varied from 12 to 32 mil.

The developed equations show good agreement to known CPW equations in the asymptotic limit.

26 September 2001
Electronics Letters Online No: 20011032
DOI: 10.1049/el:20011032

D. Jessie and L. Larson (*Department of Electrical and Computer Engineering, University of California San Diego, La Jolla, California, USA 92093*)

References

1 GHIONE, G., and NALDI, C.U.: 'Coplanar waveguides for MMIC applications: effect of upper shielding, conductor backing, finite-extent ground planes, and line-to-line coupling', *IEEE Trans. Microw. Theory Tech.*, 1987, **MTT-35**, (3), pp. 260–267

2 PONCHAK, G.E., TENTZERIS, E.M., and KATEHI, L.P.B.: 'Characterization of finite ground coplanar waveguide with narrow ground planes', *Int. J. Microcircuits Electron. Packag.*, 1997, **20**, (2), pp. 167–172

3 WENTWORTH, S.M., NEIKIRK, D.P., and BRAHCE, C.R.: 'The high-frequency characteristics of tape automated bonding (TAB) interconnects', *IEEE Trans. Compon. Hybrids Manuf. Technol.*, 1989, **12**, (3), pp. 340–347

4 VEYRES, C., and HANNA, V.F.: 'Extension of the application of conformal mapping techniques to coplanar lines with finite dimensions', *Int. J. Microcircuits Electron. Packag.*, 1980, **48**, pp. 47–56

5 GUPTA K.C., GARG, R., BAHL I., and BHARTIA, P.: 'Microwave and slotlines' (Addison-Wesley Publishing Company, New York, 1992), 2nd edn.

Linearised InGaP/GaAs HBT MMIC power amplifier with active bias circuit for W-CDMA application

Y.S. Noh and C.S. Park

A high linearity InGaP/GaAs heterojunction bipolar transistor (HBT) monolithic microwave integrated circuit (MMIC) power amplifier is demonstrated using a new structure for a bias circuit for wideband-code division multiple access (W-CDMA) application. A one shunt capacitor is added to a novel active bias circuit and acts as a linearizer improving input P_{1dB} of 16 dB and phase distortion of 5.1° for the hybrid phase shift keying (HPSK) modulated signal at the 28 dBm output power; the linearizer showing no significant increase of signal loss and chip area. The two-stage HBT MMIC amplifier exhibits a power-added efficiency (PAE) of 37%, a linear power gain of 24.5 dB, and an output power of 28 dBm with an adjacent channel power ratio (ACPR) of −45 dBc, under a 3 V operation voltage.

Introduction: A monolithic microwave integrated circuit (MMIC) power amplifier is one of the key components in mobile communication terminals, determining power consumption and thus the battery life of handsets. Power amplifiers have reduced in size, supply voltage and quiescent current. The modulation technique of wideband-code division multiple access (W-CDMA) has adopted hybrid phase shift keying (HPSK) modulation and a HPSK modulated signal has inevitably a non-constant envelope, therefore power amplifiers of high linearity are required in the transmitter system. To obtain both high power-added efficiency (PAE) and low nonlinear distortions, several methods of on-chip linearisation techniques that keep the bias of the amplifier as designed up to an input power as large as possible have been reported [1, 2]. These linearisation techniques improved output power around 0.5 dB, phase distortion of 2.2° and adjacent channel power ratio/adjacent channel leakage ratio (ACPR/ACLR) around 3.6 dB. In this Letter we propose a new linearisation technique for an InGaP/GaAs heterojunction bipolar transistor (HBT) MMIC power amplifier that improves input P_{1dB} of 16 dB and phase distortion of 5.1° for the HPSK modulated signal at the 28 dBm output power. This dramatic improvement was realised by controlling the base bias of the amplifier simply by adding a linearising shunt capacitor to a noble active bias circuit, and more importantly without increase of chip size.

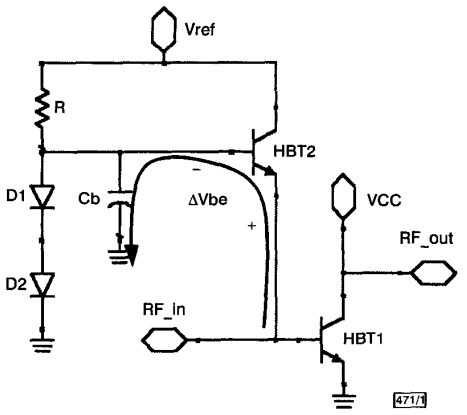

Fig. 1 *Schematic diagram of active bias circuit with linearising capacitor Cb*

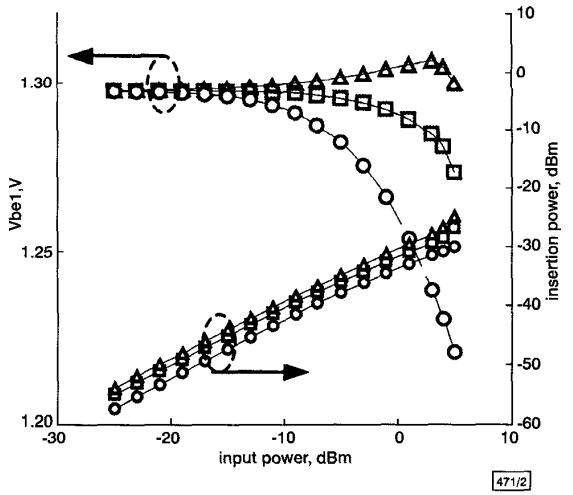

Fig. 2 *Vbe1 of HBT1 and insertion power loss to bias circuit for different values of linearising capacitance of Cb (simulation)*

—△— Cb = 6 pF
—□— Cb = 4 pF
—○— Cb = 2 pF

New linearisation technique: Our new linearisation circuit comprises a base emitter diode of an active transistor (HBT2) and a shunt capacitor (Cb) at the base of the HBT2 (Fig. 1). Without the capacitor Cb, the impedance to the bias circuit is much higher than the input impedance of HBT1, therefore almost all RF input signals enter the RF amplifier HBT1, and the base-emitter bias voltage of HBT1 becomes a decreasing function of increasing RF input signal, resulting in severe nonlinear distortions (AM-AM and AM-PM). To reduce nonlinear distortions, base bias voltage of the HBT1 is needed to maintain a constant value. The shunt capacitor (Cb) reduces input impedance towards the linearizer at